



Toward an Empirical Theory of Pulsar Emission. XII. Exploring the Physical Conditions in Millisecond Pulsar Emission Regions

Joanna M. Rankin^{1,2}, Anne Archibald^{2,3}, Jason Hessels^{2,3}, Joeri van Leeuwen^{2,3}, Dipanjan Mitra^{1,4,5}, Scott Ransom⁶,
Ingrid Stairs⁷, Willem van Straten⁸, and Joel M. Weisberg⁹

¹ Physics Department, University of Vermont, Burlington, VT 05405, USA; Joanna.Rankin@uvm.edu

² Anton Pannekoek Institute for Astronomy, University of Amsterdam, Science Park 904, 1098 XH Amsterdam, The Netherlands

³ ASTRON, the Netherlands Institute for Radio Astronomy, Postbus 2, 7990 AA, Dwingeloo, The Netherlands

⁴ National Centre for Radio Astrophysics, Ganeshkhind, Pune 411 007, India

⁵ Janusz Gil Institute of Astronomy, University of Zielona Góra, ul. Szafrana 2, 65-516 Zielona Góra, Poland

⁶ National Radio Astronomy Observatory, Charlottesville, VA 29201, USA

⁷ Physics Department, University of British Columbia, V6T 1Z4, BC, Canada

⁸ Institute for Radio Astronomy & Space Research, Auckland University of Technology, Auckland 1142, New Zealand

⁹ Physics & Astronomy Department, Carleton College, Northfield, MN 55057, USA

Received 2016 October 13; revised 2017 June 16; accepted 2017 June 19; published 2017 August 9

Abstract

The five-component profile of the 2.7 ms pulsar J0337+1715 appears to exhibit the best example to date of a core/double-cone emission-beam structure in a millisecond pulsar (MSP). Moreover, three other MSPs, the binary pulsars B1913+16, B1953+29, and J1022+1001, seem to exhibit core/single-cone profiles. These configurations are remarkable and important because it has not been clear whether MSPs and slow pulsars exhibit similar emission-beam configurations, given that they have considerably smaller magnetospheric sizes and magnetic field strengths. MSPs thus provide an extreme context for studying pulsar radio emission. Particle currents along the magnetic polar flux tube connect processes just above the polar cap through the radio-emission region to the light-cylinder and the external environment. In slow pulsars, radio-emission heights are typically about 500 km around where the magnetic field is nearly dipolar, and estimates of the physical conditions there point to radiation below the plasma frequency and emission from charged solitons by the curvature process. We are able to estimate emission heights for the four MSPs and carry out a similar estimation of physical conditions in their much lower emission regions. We find strong evidence that MSPs also radiate by curvature emission from charged solitons.

Key words: pulsars: general – pulsars: individual (J0337+1715, J1022+1001, B1913+16, B1953+29) – radiation mechanisms: non-thermal

1. Introduction

Millisecond pulsar (MSP) emission processes have remained enigmatic despite the very prominence of MSPs as indispensable tools of contemporary physics and astrophysics. MSP magnetospheres are much more compact ($\sim 100\text{--}3000$ km), and their magnetic field strengths are typically $10^3\text{--}10^4$ times weaker and probably more complex than those of normal pulsars, which is a result of the period of accretion that is believed to recycle old pulsars into MSPs.

Normal pulsars are found to exhibit many regularities of profile form and polarization that together suggest an overall beam geometry comprised by two distinct emission cones and a central core beam. It would seem that these regularities occur in the main part because the magnetic field is usually highly dipolar at the roughly 500 km height where radio emission occurs (J. M. Rankin et al. 2017, in preparation).

The vast majority of MSPs shows no such regularity. Their polarized profile forms are often broad and complex and seem almost a drunken parody of the order that is exhibited by many slower pulsars (e.g., Dai et al. 2015 and the references therein). The reasons for this disorder are not yet fully clear, but the smaller magnetospheres of MSPs may well entail emission heights where the magnetic fields are dominated by quadrupoles and higher terms. In addition, aberration/retardation (hereafter A/R) becomes ever more important for faster pulsars. In this context, it is arresting to encounter a few

MSPs that appear to exhibit the regular profile forms and perhaps polarization of normal pulsars. If so, even a few such MSPs provide an opportunity to work out their quantitative emission geometry and assess whether their radiative processes are similar to those of normal pulsars.

The profile of MSP J0337+1715 surprisingly has what appears to be a five-component core/double-cone configuration. Such a five-component structure is potentially important because it has not been clear whether MSPs ever exhibit emission-beam configurations similar to those of slower pulsars. J0337+1715 is now well known as the unique example so far of an MSP in a system of three stars (Ransom et al. 2014). The pulsar is relatively bright and can be observed over a large frequency band, so that both its pulse timing and polarized profile characteristics can be investigated in detail.

In addition, we find three other probable examples of MSPs with core-cone profiles: the original binary pulsar, B1913+16; the second MSP discovered, B1953+29; and pulsar J1022+1001. We also discuss the profile geometries of these three MSPs and consider their interpretations below.

The slow pulsars with four-component profiles show outer and inner pairs of conal components, centered closely on the (unseen) longitude of the magnetic axis, all with particular dimensions relative to the angular size of the pulsar's magnetic (dipolar) polar cap. The classes of pulsar profiles and their quantitative beaming geometries are discussed in

Rankin (1983, hereafter ET I; 1993a, 1993b, hereafter ET VIa & ET VIb) and other population analyses have come to similar conclusions (e.g., Gil et al. 1993 Mitra & Deshpande 1999; Mitra & Rankin 2011). Core beams have intrinsic half-power angular diameters about equal to a pulsar’s (dipolar) polar cap ($2.45P^{-1/2}$, where P is the pulsar rotation period), suggesting generation at altitudes just above the polar cap. Conal beam radii in slow pulsars also scale as $P^{-1/2}$ and reflect emission from heights of several hundred km. Core emission heights are not usually known apart from the low-altitude implication of their widths—so it is plausible to assume that core radiation arises from heights well below that of the conal emission.

Classification of profiles and quantitative geometrical modeling provides an essential foundation for understanding pulsars physically. MSPs, heretofore, have seemed inexplicable in these terms. The core/double-cone model works well for most pulsars with periods longer than about 100 ms, whereas faster pulsars mostly either present inscrutable single profiles or complex profiles where no cones or core can be identified. It is then important to learn how and why it is that the core/double-cone beam model often breaks down for the faster pulsars.

A/R becomes more important for faster pulsars and MSPs simply because their periods are shorter relative to A/R temporal shifts. The role of A/R in pulsar emission profiles was first described by Blaskiewicz et al. (1991, hereafter BCW), but only later was this understanding developed into a reliable technique for determining pulsar emission heights (e.g.,

Dyks et al. 2004; Dyks 2008; Mitra & Rankin 2011; Kumar & Gangadhara 2012). A/R has the effect of shifting the profile earlier and the polarization-angle (hereafter PPA) traverse later by equal amounts,

$$\Delta t = \pm 2h_{\text{em}}/c, \quad (1)$$

where h_{em} is the emission height (above the center of the star), such that the magnetic axis longitude remains centered in between. In that the PPA inflection is often difficult to determine, A/R heights have also been estimated by using the core position as a marker for the magnetic axis longitude, as first suggested by Malov & Suleimanova (1998) and Gangadhara & Gupta (2001) and now widely used. The A/R method has thus usually been used to measure conal emission heights, but core heights have also been estimated for B0329+54 (Mitra et al. 2007) and recently for B1933+16 and several other pulsars (Mitra et al. 2016), giving heights around or a little lower than the conal heights. Crucially, A/R measurements indicate emission heights of some 300–500 km in the slow pulsar population. So it is important to see how MSPs compare, given that many have magnetospheres smaller than 500 km.

In what follows we discuss the observations in Section 2, the J0337+1715 core component and its width in Section 3.1, and the conal component configuration in Section 3.2. Section 3.3 treats its quantitative geometry, Section 3.4 computes A/R emission heights, and Section 4 considers three other MSPs with cone/single-cone profiles. Finally, Section 5 summarizes the results, Section 6 interprets them physically, and Section 7 outlines the overall conclusions.

Table 1
Properties of the Arecibo and GBT Observations

Band (GHz)	Backend	MJD	Resolution (°/sample)	Length (s)
<i>J0337+1715</i> ($P = 2.73$ ms; $DM = 21.32$ pc cm $^{-3}$)				
1.1–1.7	PUPPI	56736	0.70	~3400
1.1–1.8	GUPPI	56412	0.70	40,968
0.42–0.44	PUPPI	56584	1.41	~3400
1.9–2.5*	PUPPI	56781	1.41	3600
1.9–2.5	PUPPI	57902	1.41	3600
2.5–3.1*	PUPPI	56768	1.41	3936
2.5–3.1	PUPPI	57902	1.41	3000
1.1–1.7	Mocks	56760	4.74	1000
<i>B1913+16</i> ($P = 59.0$ ms; $DM = 168.77$ pc cm $^{-3}$)				
1.1–1.9	GUPPI	55753	0.35	1900
1.1–1.7	Mocks	56199	0.58	1200
<i>B1953+29</i> ($P = 6.13$ ms; $DM = 104.501$ pc cm $^{-3}$)				
1.1–1.6	Mocks	56564	2.24	2400
1.1–1.6	Mocks	56585	2.24	2400
1.1–1.9	PUPPI	57129	0.35	3608
<i>J1022+1001</i> ($P = 16.4$ ms; $DM = 10.2521$ pc cm $^{-3}$)				
1.1–1.7	Mocks	56315/23	0.53	600
1.1–1.7	Mocks	56577	0.46	1800
0.30–0.35	Mocks	56418/31	2.55	600
0.30–0.35	Mocks	56577	2.55	1800

Note. These earlier PUPPI 2.0 and 2.8 GHz observations could not be calibrated polarimetrically because of faulty cal signals; therefore, we use only Stokes I in Figure 5.

2. Observations

2.1. Acquisition and Calibration

J0337+1715. A large number of observations at different frequencies and observatories were carried out in the course of confirming J0337+1715 and understanding the complex orbital modulations of its pulse-arrival times. Some of these were polarimetric and some much more sensitive, and unsurprisingly, the Arecibo observations were usually of the highest quality. In compiling the observations for this analysis, we assessed which observations were deepest at both 1400 and 430 MHz. The PUPPI backend¹⁰ was used at both frequencies with a 30 MHz bandwidth at 430 and a 600 MHz bandwidth at 1400 MHz. We then explored the pulsar’s behavior at higher frequencies, and both 2.0 and 2.8 GHz observations are reported here. We also attempted a rise-to-set observation at 5 GHz with a 1 GHz bandwidth, but the pulsar was not detected. All the J0337+1715 observations were calibrated or recalibrated using the PSRchive *pac-x* routine (Hotan et al. 2004). The final bin size was chosen to reflect the joint time and frequency resolution, and is given in Table 1 along with some other characteristics of the observations.

The 1391 MHz profile in Figure 1 is the deepest and best resolved of the four and deserves more detailed analysis. The 2.8, 2.0, and 0.43 GHz profiles can be seen in Figure 2.

B1913+16, B1953+29, and J1022+1001. We also carried out Arecibo observations of these pulsars using the L-band Wide feed and the Mock¹¹ spectrometers. The former were single-pulse polarimetric observations using as many Mock spectrometers as needed to optimize the resolution and use the

¹⁰ <http://www.naic.edu/~astro/guide/node11.html>

¹¹ <http://www.naic.edu/~astro/mock.shtml>

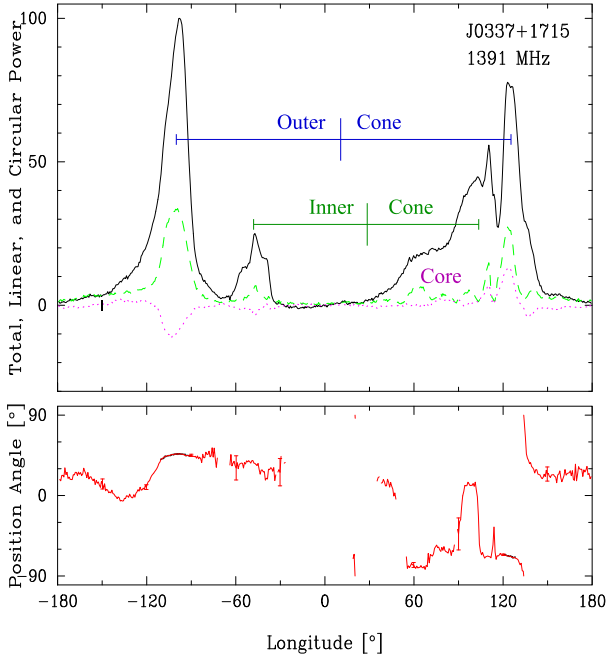


Figure 1. Total 1.4 GHz Arecibo PUPPI polarized profile of pulsar J0337+1715 showing its apparent core component as well as its pairs of inner and outer conal components. The core component seems to be conflated with the trailing conal components at about 90° longitude. The positions and centers of the two conal component pairs are indicated. They are far from symmetrically spaced as in slower pulsars, apparently because of aberration/retardation. However, note that the outer cone center precedes the inner one as well as the core. The upper panel gives the total intensity (Stokes I ; solid curve), the total linear ($L[=\sqrt{Q^2 + U^2}]$; dashed green), and the circular polarization (Stokes V ; dotted magenta) have been Faraday-derotated to infinite frequency. The PPA $[=(1/2)\tan^{-1}(U/Q)]$ values (lower panel) have been Faraday-derotated to infinite frequency. Errors in the PPAs were computed relative to the off-pulse noise phasor—that is, $\sigma_{\text{PPA}} \sim \tan^{-1}(\sigma_{\text{off-pulse}}/L)$ and are plotted when $<30^\circ$ and indicated by occasional 3σ error bars.

total available bandwidth for maximum sensitivity, and the results are given in Table 1. These Mock observations were processed as described in Mitra et al. (2016), including derotation to infinite frequency.

2.2. Rotation-measure (RM) Determinations

Our RM determinations will be published as a part of a larger paper in preparation together with a full description of our observations and techniques.

J0337+1715. A RM of $+30 \pm 3 \text{ rad m}^2$ was determined using a set of the best-quality observations from both the Arecibo PUPPI and Green Bank Telescope (hereafter GBT) GUPPI machines.¹² These were processed as above with PSRchive, and its rmfit routine was used to estimate each RM and its error; the stated error then reflects the scatter of these values. Ionospheric corrections estimated for these observations ran between $+0.8$ and -0.2 rad m^2 , so the intrinsic value lies well within the above error. Separately, the Mock observation of MJD 56760 was used to determine an ionosphere-corrected value of $+29.3 \pm 0.7 \text{ rad m}^2$.

B1913+16. An accurate RM value was determined for the first time using five Arecibo Mock 1.4 GHz observations—one of which is shown below in Figure 3. After ionospheric

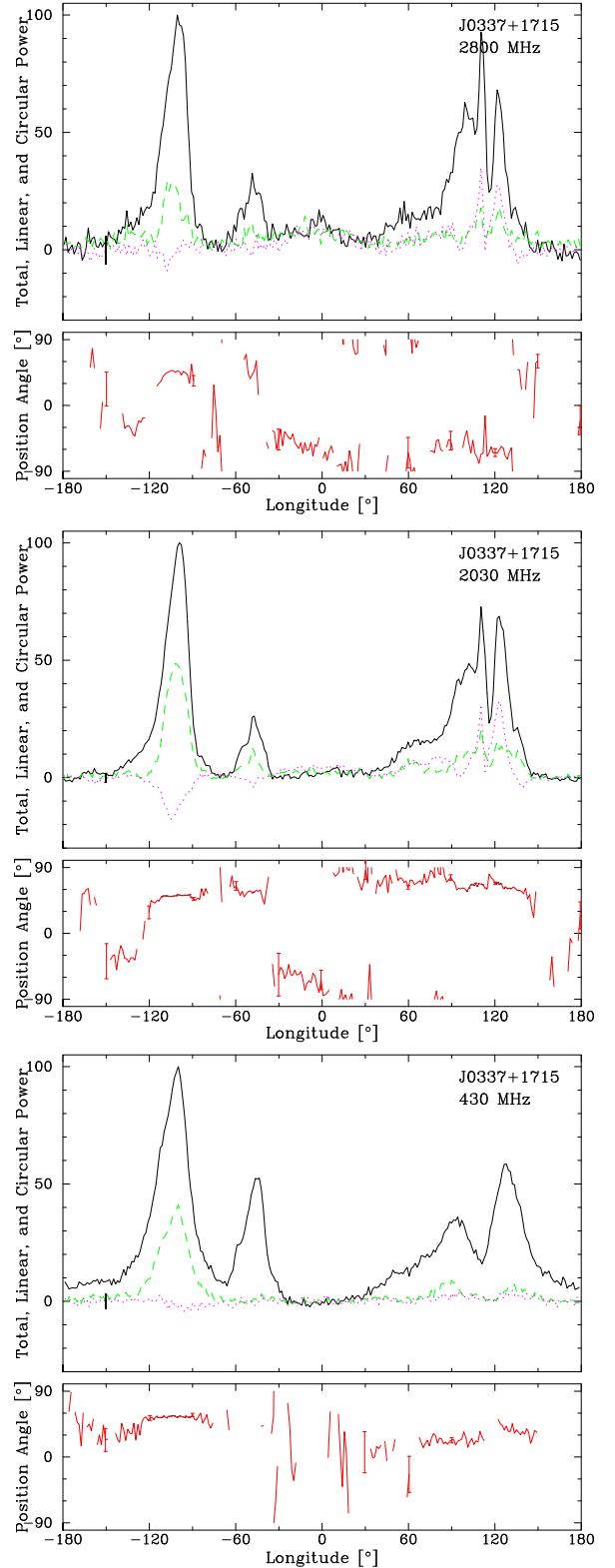


Figure 2. Arecibo PUPPI profiles of J0337+1715 after Figure 1 at higher and lower frequencies than the earlier 1391 MHz profile; see Table 1. These show the near absence of evolution with frequency. The profiles, as well as that at 1.4 GHz above, are aligned with the dispersive delay removed.

¹² <https://safe.nrao.edu/wiki/bin/view/CICADA/GUPPIUsersGuide>

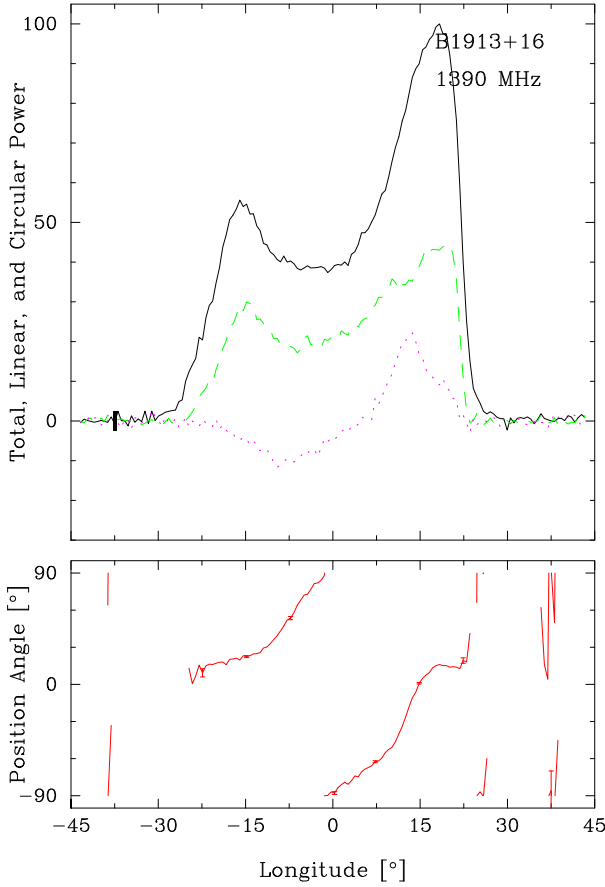


Figure 3. Arcibo 1.4 GHz Mock spectrometer profile of B1913+16 from 2012 September 29. The form of this profile differs substantially from those measured earlier (e.g., BCW) because of the star’s precession. This observation was carried out with four Mock spectrometers sampling 86 MHz bandwidths and $95 \mu\text{s}$ resolution. The PPAs have been derotated to infinite frequency using the measured RM value above, ionosphere corrected, of $+354.4 \pm 0.4 \text{ rad m}^2$.

correction, the RMs were estimated by trial and error maximization of the aggregate linear polarization resulting in a value of $+354.4 \pm 0.6 \text{ rad m}^2$, where the error reflects the rms scatter of the values. This value is then further confirmed by a GBT GUPPI observation, made as part of another project (Force et al. 2015) and processed using the PSRchive rffit routine to yield an RM value of $+357.9 \pm 1.5 \text{ rad m}^2$ that included some 2–3 units of ionospheric contribution. This represents a substantial increase in precision compared to the current value on the ATNF Pulsar Catalog website of $+430 \pm 77 \text{ rad m}^2$ (Han et al. 2006).

B1953+29. This RM value was also estimated for the first time using Arcibo 1.4 GHz observations as processed by both the Mock spectrometers and PUPPI. The two Mock observations were processed as above and together yielded a value of $+3.0 \pm 0.4 \text{ rad m}^2$, corrected for ionospheric contributions; the second of the two is shown in Figure 4. In addition, a PUPPI observation was processed as above using PSRchive rffit and yielded a value of $+5.7 \pm 3.0 \text{ rad m}^2$, which was not corrected for the expected 2–3 units of ionospheric RM.

J1022+1001. This pulsar has a well-determined RM value of $+1.39 \pm 0.05 \text{ rad m}^2$ on the ATNF Pulsar Catalog website according to Noutsos et al. (2015).

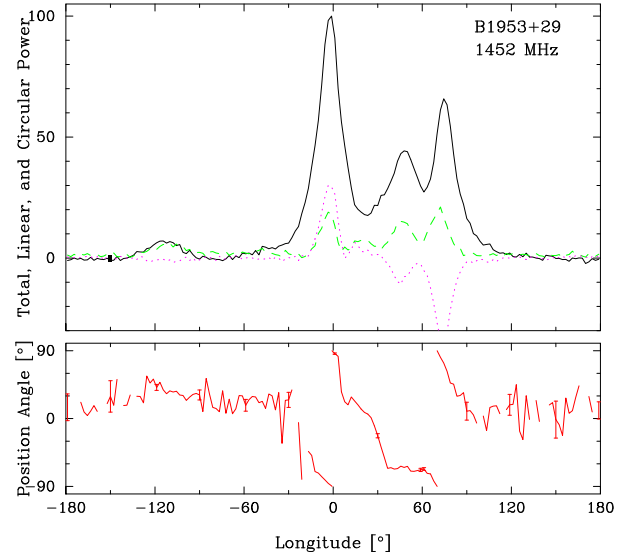


Figure 4. Arcibo 1.4 GHz Mock spectrometer profile of B1953+29 from 2013 October 20. This observation was carried out with seven Mock spectrometers sampling adjacent 34 MHz bands with a $38 \mu\text{s}$ sampling time. Note what appears to be an interpulse preceding the putative core-cone triple (*T*) main pulse. We believe this is the first observation to clearly show the pulsar’s PPA traverse and interpulse. The PPAs have been derotated to infinite frequency using its measured RM of $+2.9 \pm 0.6 \text{ rad m}^2$ (including some 0.8 rad m^2 in the ionosphere). A further Arcibo observation carried out with PUPPI confirms the profile structure and RM value.

3. Exploration of the J0337+1715 Profile

3.1. The Putative Core Feature and its Width

In slower pulsars, the core component width reflects the angular diameter of the polar cap near the stellar surface, and as such has an intrinsic half-power diameter of $2.45P^{-1/2}$ (P is the stellar rotation period), but the observed width entails a further factor of $\csc \alpha$ (where α is the colatitude of the magnetic axis with respect to the rotation axis). The expected intrinsic width for this 2.73 ms MSP would then be some 47° and the observed width 67.5° , given that α is plausibly 44° (Ransom et al. 2014) if the orbital and rotational angular momenta are aligned. In J0337+1715’s profile, the putative core is conflated with the trailing inner conal component over the entire observable band, therefore the core width can only then be estimated. Exploratory modeling of the four profiles in the Appendix suggests a core width of between 60° and 70° , so we have fixed the core width in our modeling at the above expected 67.5° observed value.

3.2. Double Cone Configuration

In slower pulsars, conal components occur in pairs for interior sightline traverses where the sightline impact angle $|\beta|$ is smaller than the conal beam radius ρ . Geometrically, these conal component pairs are found to be of two types, inner and outer cones, that have specific (outside, half-power, 1 GHz) radii ρ of $4.33P^{-1/2}$ and $5.75P^{-1/2}$ (ET VIa, ET VIb; see VIa Equation (4)). In pulsars where both cones and a core are observed, profiles then have five components, such as in pulsar B1237+25.

We suggest that pulsar J0337+1715’s profile in Figure 1 may exhibit just these five components as well as a narrow (putative caustic; see below) feature on the outer edge of the

trailing inner conal component, and we also model these features in the [Appendix](#). The leading outside (LOC) and inside conal (LIC) components are seen to fall at about -100° and -50° longitude, respectively.

The core is conflated with the trailing conal components (TIC and TOC) at some $+100^\circ$ and $+125^\circ$, as modeled and better estimated in [Table 6](#). The conal components are asymmetric and the rightmost one has a trailing edge bump. However, the [Appendix](#) modeling appears to locate their centers and half-widths adequately. The “spike” on the trailing edge of the trailing inner conal feature above 1 GHz deserves special mention, as it seems to resemble the “caustic”¹³ features that are seen in some other pulsars. The 1391 MHz polarization-angle (PPA) traverse shows what seems to be a 90° “jump” at about 135° longitude, and earlier ones at about 50° and 100° ; if these are resolved, then the PPA seems to rotate rather little under the components as seems possibly the case at the other more depolarized frequencies.

3.3. Quantitative Geometry

Profiles for frequencies both higher and lower than that in [Figure 1](#) are given in [Figure 2](#). Note that the pulsar’s five components can easily be discerned in these profiles up to 2.8 GHz and down to 430 MHz. The conal features of the 430 MHz profile are broader and appear less well resolved compared to the higher frequency profiles; however, this appears not to be the result of poorer instrumental resolution and scattering. The core is obviously conflated with the trailing inner conal component across all the observations, and this must be taken into account in identifying the structures contributing to the pulsar’s overall profile.

The centers (C), widths (W) and amplitudes (A) of J0337+1715’s components are given in [Table 6](#), where an effort was made to determine these values by fitting methods. However, given the irregular shapes of the components, the fitting errors are small compared to systematic ones of a few degrees. The table thus gives the positions and widths of the conal components so obtained as well as those of the putative “caustic” feature (CC in [Table 6](#)) whose center could be fitted within about 1° —and it is satisfying to see that this feature aligns in the high frequency profiles within this latter error. Unsurprisingly, the core component properties are more difficult to estimate in the various profiles, even when taking the widths as fixed at the expected value as shown in the table. We discuss this further below in connection with the A/R analysis where this difficulty is most pertinent.

The properties of the two cones are given in [Table 2](#), where w_i and w_o are the inner and outer outside, half-power conal widths, computed as the longitude interval between the component-pair centers plus half the sum of their widths. Here we see that the inner and outer conal widths are essentially constant over the observable frequency band. This near constancy of profile dimensions over some three octaves is similar to that observed for other MSPs where there is little change in the components separations over the total band of observations (e.g., [Kondratiev et al. 2016](#)).

Here we apply the standard spherical geometric analyses assuming a central sightline traverse (sightline impact angle β

¹³ “Caustic” refers to a field-line geometry in which an accidentally favorable curvature tracks the sightline producing a bright narrow broadband feature (e.g., [Dyks & Rudak 2003](#)).

Table 2
Double Cone Geometry Model for PSR J0337+1715

Freq (MHz)	w_i ($^\circ$)	ρ_i ($^\circ$)	w_o ($^\circ$)	ρ_o ($^\circ$)	h_i (km)	h_o (km)
2800	162	54	238	74	52	99
2080	163	54	242	74	53	101
1391	166	55	240	74	53	99
430	163	54	252	76	53	107

Note. w_i and w_o are the outside half-power inner and outer conal component widths scaled from [Figures 1](#) and [2](#). ρ_i and ρ_o are the outside half-power conal beam radii computed from [ET VIa](#), Equation (4), and h_i and h_o are the respective geometric conal emission heights computed from the latter paper’s Equation (6) assuming dipolarity and emission along the polar flux-tube boundary.

about 0° as suggested by the relatively constant PPA traverse), that the magnetic colatitude α is 44° , and that the emission occurs adjacent to the “last open field lines” (e.g., [ET VIa](#)). This analysis is summarized in [Table 2](#), where ρ_i and ρ_o are the computed conal emission beam radii (to their outside half-power points) per Equation (4) in [ET VIa](#). The emission characteristic heights are then computed assuming dipolarity using Equation (6).

The outside half-power conal radii of about 54° and 75° are of course enormous compared to those found for slow pulsars. However, they are substantially smaller—only about 2/3—what would be expected according to the slow pulsar relationships $4^\circ:33P^{-1/2}$ and $5^\circ:75P^{-1/2}$ for the outside 3 dB radii of inner and outer cones. The model emission heights of some 53 and 100 km are also correspondingly smaller—less than half of the 120 and 210 km typically seen in the slow pulsar population. However, it is important to recall that these are *characteristic* emission heights, not physical ones, estimated using the convenient but problematic assumption that the emission occurs adjacent to the “last open” field lines. It will be interesting to compare these heights with the physical emission heights estimated using A/R just below.

3.4. A/R Analysis

Here we see that the centers of the outer and inner conal component pairs precede the longitude of the core-component center by some 60° or more—and we propose to interpret this shift as due to A/R to assess whether the results are appropriate and reasonable. A difficulty is determining the position of the core component accurately, given its conflation with the outer conal components. [Table 6](#) below reports the results of modeling the pulsar’s features with Gaussian functions in order to assess the character of this conflation and then estimate the core component’s position and center. Assuming a constant core width at its expected 67.5 value and a constant amplitude in relation to the four conal components, the core center falls close to -85° in each band within about 2° . However, other modeling assumptions might well yield somewhat different values. We therefore propose to take the core center at $-85^\circ \pm 10^\circ$ in order to incorporate the major range of estimates and uncertainties. Finally, as emphasized above, core components exhibit a predictable width in slow pulsars that reflects both the polar cap geometry and the magnetic colatitude. This is the rationale for holding the core width here to its expected value. If, however, J0337

Table 3
Aberration/Retardation Analysis Results for PSR J0337+1715

Freq/Cone (MHz)	ϕ_1^i (deg)	ϕ_t^i (deg)	ϕ_c^i (deg)	κ^i (deg)	ρ^i (deg)	h_{em}^i (km)	s^i
2800/II	-105 ± 3	124 ± 4	10 ± 5	-75 ± 11	71.5 ± 1.6	86 ± 13	0.91 ± 0.07
2030/II	-102 ± 3	125 ± 4	11 ± 5	-74 ± 11	71.1 ± 1.7	84 ± 13	0.92 ± 0.07
1391/II	-100 ± 3	128 ± 4	14 ± 5	-71 ± 11	71.2 ± 1.6	81 ± 13	0.94 ± 0.07
430/II	-103 ± 3	129 ± 4	13 ± 5	-72 ± 11	72.2 ± 1.6	82 ± 13	0.94 ± 0.07
2800/I	-51 ± 2	98 ± 4	24 ± 4	-62 ± 11	49.5 ± 1.9	70 ± 12	0.74 ± 0.07
2030/I	-49 ± 2	97 ± 4	24 ± 4	-61 ± 11	48.9 ± 1.9	69 ± 12	0.74 ± 0.07
1391/I	-47 ± 2	99 ± 4	26 ± 4	-59 ± 11	48.9 ± 1.9	67 ± 12	0.75 ± 0.07
430/I	-48 ± 2	94 ± 4	23 ± 4	-62 ± 11	47.5 ± 2.0	71 ± 13	0.71 ± 0.06

Note. ϕ_1^i and ϕ_t^i are the leading and trailing conal component positions; ϕ_c^i their centers; κ^i are the total A/R shifts in longitude as marked by the core component centers; h_{em}^i the A/R emission heights computed from Equation (2); and ρ^i and s^i are the conal radii and emission annuli within the polar flux-tube computed using ET VIa Equation (4) and $\sin(2\rho^i/3)\sqrt{R_{\text{lc}}/h^i}$, respectively.

+1715, for whatever reason, had a core that was smaller or larger, then the center would shift by half the difference amount.

Table 3 below gives A/R analyses for the two cones in the four bands. The column values give the peaks of the leading and trailing conal components ϕ_1 and ϕ_t , their center point $\phi_c = (\phi_t + \phi_1)/2$, and the offsets. The total A/R shift is then given by κ , which is computed as the longitude interval between the conal centers ϕ_c and the longitude of the magnetic axis as marked by the core component, or $+85^\circ - \phi_c$, and its uncertainty is dominated by the above $\pm 10^\circ$ in the estimated core position.

The conal radii ρ corresponding to the conal component-pair peak separations are calculated geometrically as in Table 2, and those values are somewhat larger as expected, about 54° and 75° , than tabulated here, given their reference to the outside half-power points rather than the component peaks. This computation is independent of the A/R height determination and is used only to estimate the annuli of the emitting locations s^i , where 0 lies along the magnetic axis and unity on the polar flux tube boundary. That these values for the outer cone are close to unity tends to support our geometrical model assumption above that its emission regions lie on the periphery of the (dipolar) polar flux-tube; the inner cone is then emitted more to the interior and higher in altitude.

In A/R analysis here, per Equation (2), the relation

$$h_{\text{em}} = -c\phi_c P/360^\circ/2 \quad (2)$$

provides a reliable estimate of the emitting region height, subject only to correct interpretation of the core-cone beam structure and determination of the core component's position as marking the magnetic axis longitude or a region just above it—in any case at a much lower altitude than the conal emission. The resulting physical A/R emission heights for the inner and outer cones are then about 70 km and 85 km, respectively, where the velocity-of-light-cylinder distance is $R_{\text{lc}} (=cP/2\pi)$ 130 km. We find no significant emission-height differences over the nearly three octaves of observations. This analysis parallels those for slower pulsars in Force & Rankin (2010), Mitra & Rankin (2011), Smith et al. (2013), and most recently, Mitra et al. (2016), and are based on BCW as corrected by Dyks et al. (2004).

4. Apparent Core-cone Beam Structure in Other MSPs

4.1. B1913+16

The binary pulsar B1913+16 has been studied intensively using timing methods, resulting in the identification of gravitational radiation (e.g., Weisberg & Huang 2016), but until recently, the pulsar was difficult to study polarimetrically. Moreover, the star precesses causing secular changes in its profile and polarization (e.g., Weisberg & Taylor 2002). However, its early basic profile morphology had been known to be tripartite at 430 MHz and double at 1400 MHz and above. This is just as seen in many slow pulsars, and one of us classified this pulsar as having a core/inner-cone triple (T) profile (ET VIb) on the basis of the 430- and 1400 MHz profiles then recently published by Blaskiewicz et al. (1991 their Figure 17). These profiles show a typical evolution due to the core's relatively steep spectrum—such that in B1913+16 the core is not resolvable at frequencies above 1 GHz. Key to understanding the central component as being a core is its width, which reflects the angular size of the star's polar cap at $2.45P^{-1/2}$ or 10° intrinsically and then broader by a factor of $\csc\alpha$ in profile longitude. Our Gaussian fit to the 1990 430 MHz profile in Figure 7 gives a value of $17^\circ \pm 2^\circ$, which supports both the core identification and an α value of about 45° as in ET VIa and ET VIb (where the 1 GHz width is taken as 14° . This in turn is quite reasonable if the star's spin and orbital rotations were aligned, but the pulsar's precession shows that they are not. The star's changing profile forms at 430 MHz suggest a core/cone beam moving toward and ever less central sightline traverse, greatly complicating models of its emission geometry.¹⁴

We then take the geometric model in ET VIb, Table 4, based on profiles reported by BCW—at a time when the 430 MHz core was most clearly seen—as close to the mark for our purposes here. Its central sightline traverse makes it insensitive to β . Similarly, the 430 MHz profile is broader at the conal outside half-power points, but the conal peak separation is nearly constant at about 40° between the two frequencies, so the increased breadth must be intrinsic and the cone thus an inner one. Therefore, we confirm the core/inner-cone geometry of ET VIa and ET VIb.

¹⁴ Some precession models suggest lower α values (Kramer 1998; Weisberg & Taylor 2002; Clifton & Weisberg 2008), but both the core and conal widths seem too narrow to support this. Such models incur their own assumptions and difficulties such that the differences between methods are not easily reconciled.

Table 4
Conal Geometry Models for B1913+16, B1953+29 and J1022+1001

Pulsar	P (ms)	α ($^\circ$)	β ($^\circ$)	w ($^\circ$)	ρ ($^\circ$)	h (km)
B1913+16	59.0	46	4.0	47	17	126
B1953+29	6.1	>65	-18	100	44.4	81
J1022+1001	16.4	\sim 60	\sim 7	42	20	45

Note. P , α , and β are the pulsar’s rotation period, magnetic colatitude, and sightline impact angle, respectively. The w s are the outside half-power conal component widths measured from the fitting of Figures 7–9. The ρ s are the outside half-power conal beam radii computed from ET VIa, Equation (4), and the h s are the respective geometric conal emission heights computed from the above Equation (6) assuming dipolarity and emission along the polar flux-tube boundary.

BCW pioneered the use of A/R for determining pulsar emission heights, and their analysis for B1913+16 is illustrated in their Figure 17. They determined the A/R shift from the PPA steepest gradient point (SG) backward to the center of the conal component pair. Arrows in the figures show these points, and according to their analysis, the A/R shift, averaged between the two frequencies, is 12.5 ± 1.0 , which then corresponds to an emission height of 126 ± 21 km. This in turn then occurs within a light-cylinder radius of 2820 km.

If the above two points are well identified, the above A/R value follows the method BCW advocated. We can then try to estimate the emission height by two other methods: first, the fits in Figure 7 clearly show that the core component peak lags the center point between the two conal peaks, and this lag is 1.5 or 0.246 ms or some 37 km in altitude per Equation (1)—that is, the conal emission region appears to be higher than the core region by this amount. Second, the zero-crossing point of antisymmetric circular polarization often marks the longitude of the magnetic axis,¹⁵ and in the B1913+16 profile of Figure 3 this point falls $6^\circ \pm 1^\circ$ or some 1.0 ms after the conal center point, suggesting a conal emission height of 148 ± 25 km. As the magnetic axis longitude falls halfway between the oppositely shifted profile and PPA traverse under A/R, the latter result is compatible with BCW’s interpretation and the 37 km shift may represent the height between the core and conal emission regions.

4.2. B1953+29

The second MSP, B1953+29, also known as Boriakoff’s pulsar (Boriakoff et al. 1983), is also a binary pulsar with a 117-day orbit. It has also had little subsequent study because few profiles have been measured in the intervening decades. Profiles and provisional polarimetry at both 430 and 1400 MHz were presented at an NRAO workshop just after the discovery (Boriakoff et al. 1984), but were not otherwise published, and the polarimetry efforts appearing since (Thorsett & Stinebring 1990; Xilouris et al. 1998; Han et al. 2009; Gonzalez et al. 2011) leave many questions unanswered. The pulsar was difficult to observe polarimetrically, but Arecibo’s L-band Wide feed together with the Mock spectrometers or PUPPI now permit much more sensitive and resolved observations.

¹⁵ Core components in slow pulsars often exhibit antisymmetric circular polarization, such that the zero-crossing point marks the longitude of the magnetic axis. No core is resolvable in Figure 3, but the “bridge” region between the two conal peaks is probably dominated by core emission.

The 430 MHz profile described by Boriakoff et al. is single, showing only weak inflections from power in conal outriders on both sides of the broad and relatively intense central component. At the higher frequency, however, all three components are visible and distinct. This is just the evolution seen for most conal single (S_7) pulsars as first described in Rankin (ETI, ET VIa). No full beamform computation was given for the pulsar in ETVIb because no reliable polarimetry was then available.

Figure 4 shows a recent Arecibo 1452 MHz polarimetric observation conducted with the Mock spectrometers. It is far more sensitive and better resolved than any previously published polarimetry for this important pulsar, and clearly shows its PPA traverse as well as what appears to be a bright interpulse.¹⁶ Again, we have little basis for proceeding with our interpretation of the B1953+29 profile unless its putative core component shows an adequate width reflecting that of the polar cap. For this 6.1 ms pulsar, the intrinsic core width $2.45P^{-1/2}$ (ET VIa, Equation (2)) is expected to be some 31.3 . Fits to the central component discussed in the Appendix give a width of 34.5 with a fitting error of less than a degree. The larger error here, however, is systematic: a Gaussian function may not fit the core feature well and the adjacent overlapping components imply significant correlations. The fitting then indicates a core width that is unlikely to be larger than the fitted value but possibly slightly smaller. Thus there is strong indication that this is a core, and that the width reflects a magnetic colatitude—via the $\csc\alpha$ factor—close to orthogonal, that is, some 65° or more. The leading feature (preceding the core by about 163°) would then support a nearly orthogonal geometry if indeed this is an interpulse—and we will make this assumption.¹⁷

Now we can also see from Figure 4 that the PPA rate is about $-3^\circ/^\circ$. Following the quantitative geometric analysis of ET VIa and ET VIb using the profile dimensions (see the Appendix and Table 7), the results are given in Table 4, where for a magnetic colatitude α of 65° the characteristic emission height would be only some 81 km (rather than the 110–120 km typical of inner-cone characteristic heights of normal pulsars). An A/R analysis of the B1953+29 profile, assuming that the core component is at the longitude of the magnetic axis, results in the conclusion that the conal center precedes the core by $11^\circ \pm 3^\circ$, and this in turn corresponds a relative core-cone emission height difference of 27 ± 5 km within a light-cylinder radius of 293 km.

4.3. J1022+1001

PSR J1022+1001, discovered by Camilo et al. (1996), is a recycled MSP with a rotation period of 16 ms. It is in a binary system with an orbital periodicity of 7.8 days. The pulsar has been part of several long-term timing programs, but is well known to time poorly.¹⁸ It has been observed over a broad frequency band, (e.g., Dai et al. 2015; Noutsos et al. 2015), and below 1 GHz, its profile is clearly comprised of three prominent components. The underlying PPA traverse has a characteristic S-shaped RVM form with a “kink” under the

¹⁶ This interpulse is also clearly seen in the timing study of Gonzalez et al. (2011)—and hinted at in some of the earlier profiles—and their unpublished arxiv profile agrees well with ours here.

¹⁷ The unusual 360° total PPA rotation also suggests an inner (that is poleward) sightline traverse.

¹⁸ However, with adequate calibration, the pulsar has recently been shown to time well (van Straten 2013).

central component similar to that seen in B0329+54 by Mitra et al. (2007), such that the central slope is some $7^\circ/^\circ$ (Xilouris et al. 1998; Stairs et al. 1999). Some studies argue that the pulsar exhibits profile changes on short timescales, an effect perhaps similar to mode changing in normal pulsars (see Kramer et al. 1999; Ramachandran & Kramer 2003; Hotan et al. 2004 and Liu et al. 2015). Our three pairs of Arecibo observations at 327 and 1400 MHz also suggest slightly different linear and circular polarization at different times while confirming the basic profile structures seen in the above papers and the star’s profiles shown here.

In Figure 9 we show Gaussian component fits to J1022+1001 using profiles from Stairs et al. (1999) (Jodrell Bank profiles downloadable from the European Pulsar Network database¹⁹). We find that these profiles can be decently fitted with three components, the central one having a width of 17° at 610 MHz and 14° at 410 MHz, roughly close to the polar cap size of 19° . In these fits the location and width of the leading component are highly correlated and cannot be constrained very well, with some effect also on the central component. This said, the effect of A/R in terms of the core center lagging the center of the overall profile is clearly seen in this pulsar. The magnitude of this lag is about 6.5° at 410 MHz and 7° at 610 MHz, where we find the center of the overall profile based on the outer Gaussian-fitted component half-power points in Table 7. These estimates place the conal emission at about 20 km above the core emission.

In a short communication, Mitra & Seiradakis (2004) used an A/R model to estimate the emission height across the pulse. They argued that the pulsar could be interpreted in terms of a central core and a conal component pair as shown in their Figure 2. They found a slight difference in emission height between the core and conal emission, which then had the effect due to A/R of inserting a kink in the PPA traverse similar to what is observed. For this to happen, they suggest that the core emission originates closer to the neutron star surface, and the conal emission region is then about 25 km above that of the core emission, similar to estimates obtained from the profile analysis mentioned above.

5. Summary of Observational Results

MSP J0337+1715 apparently provides a rare opportunity to study a core/double-cone emission beam configuration in the recycled and relatively weak magnetic field system of an MSP. Slow pulsars with five-component profiles showing the core and both conal beams are unusual—because our sightline must pass close to the magnetic axis to encounter the core and resolve the inner cone—but such stars exhibit the most complex beamforms that pulsars normally seem capable of producing.

The conal dimensions of J0337+1715 and A/R analysis provide a novel and consistent picture of the emission regions in this MSP. The A/R analysis argues that the inner conal emission is generated at a height of some 70 km and the outer cone then at about 85 km, and adjustment of the quantitative geometry for the estimated s_L values provides roughly compatible emission heights. No evidence of conal spreading is seen over the nearly three octave band of observations, again suggesting that all the emission is produced within a narrow range of heights.

Questions have remained about whether MSPs radiate in beamforms similar to those of slower pulsars. When putative core components have been seen in MSPs—as in the roughly five-component profiles of J0437–4715—they are usually narrower than the polar-cap angular diameter and thus cannot be core emission features in the manner known from the slow pulsar population. This might be because MSP magnetic dipoles are not centered in the star, which in turn might result from the field destruction during their accretional spinup phase (e.g., Ruderman 1991). Or conversely, perhaps in J0337+1715 this field destruction was more orderly or less disruptive than in many other MSPs.

Core/cone beam structure had heretofore been identified in a few MSPs—B1913+16, B1953+29, and J1022+1001—and not systematically assessed in these until recently because the available polarimetry made quantitative geometric modeling difficult and inconclusive. Here we have been able to carry out such analyses that argue strongly for core/cone structure in these three other MSPs. In each case, we find core widths that are compatible with the full angular size of their (dipolar) polar caps at the surface. We further find characteristic emission heights for these pulsars that are all smaller or much smaller than expected for the inner cones of normal pulsars. A/R analyses then provide more physical emission heights: For B1913+16, a 59 ms MSP with the largest light-cylinder of 2820 km, its properties are most like those of slow pulsar inner cones. For each of the other three, however, with much faster rotations and smaller magnetospheres, both the quantitative geometry and A/R analyses indicate radio emission from lower altitudes of only a few stellar radii.

These results can embolden us to recognize core/cone structure in other MSPs, classify them, and study their emission geometry quantitatively in order to determine if, in fact, some few other core/cone profiles can be recognized among the many MSPs with inscrutable ones. These results underscore that while the few MSPs here seem to exhibit such structure, many or most appear not to. Thus these results may begin to provide a foundation for exploring the consequences of accretional magnetic field destruction during MSP spinup. It may well be that orderly core/cone beam structure signals and depends on a nearly dipolar magnetic field configuration at the height of the radio-emission regions (J. M. Rankin et al. 2017, in preparation). Therefore, for reasons to be learned in the future, some MSPs may be able to retain a sufficiently dominant dipolar magnetic field in their radio emission regions despite its dramatic weakening by accretion—whereas most other MSPs apparently do not.

6. Physical Analysis of Emission-region Conditions

Other recent A/R analyses of slower pulsars (e.g., Mitra et al. 2016 and references therein), and theoretical developments (e.g., Gil et al. 2004; Melikidze et al. 2014 and references therein) strongly argue that the radio emission in slower pulsars comes from altitudes of about 500 km. By then estimating the magnetic field strength, the Goldreich-Julian (1969) plasma density $n_{GJ} = \Omega \cdot B / 2\pi c$ (rotational frequency $\Omega = 2\pi/P$, B is the magnetic field, and c the light speed), and the plasma, cyclotron, and curvature frequencies at these heights of emission, we are able to show that the radiation emerges from regions where the three latter frequencies are all much greater than the frequency of the emitted radiation. This indicates that the mechanism of radiation must be the curvature

¹⁹ <http://www.epta.eu.org/epndb/>

Table 5
Summary of Plasma Properties for MSP Radiation

Pulsar	P (ms)	\dot{P} (10^{-20} s s $^{-1}$)	Beamform	ν_{obs} (GHz)	h (km)	ν_B (GHz)	ν_p (GHz)	ν_{cr} (GHz)	R	R_{lc} (km)
J0337+1715	2.732	1.76	Inner Cone	1.4	69	19	15–146	11–87	0.53	130
			Outer Cone	1.4	83	11	11–111	10–79	0.64	130
B1913+16	59.0	86	Inner Cone	1.4	126	101	7–73	2–14	0.04	2817
B1953+19	6.13	2.97	Inner Cone	1.4	27	614	55–555	12–93	0.09	293
				<i>81</i>	<i>23</i>	<i>11–107</i>	<i>7–54</i>	<i>0.28</i>	<i>293</i>	
J1022+1001	16.4	4.3	Inner Cone	1.4	25	1530	53–535	7–59	0.03	786
				<i>45</i>	<i>262</i>	<i>22–221</i>	<i>5–44</i>	<i>0.06</i>	<i>786</i>	

Note. The frequency ν_B is the cyclotron frequency estimated for $\gamma_s = 200$, frequency ν_p estimated for $\gamma_s = 200$ and two values of $\kappa = 100, 10^4$, and the cyclotron frequency estimated for two values of $\Gamma_s = 300, 600$. Italicized values follow from the geometric model (characteristic) heights in Table 4.

process and the emitting entities charged solitons (e.g., Mitra et al. 2009, 2015, 2016; Mitra & Rankin 2017), which in turn connects with constraints on the physical propagation modes (ordinary, extraordinary) of the observed radiation (Rankin 2015).

We then here assess the results of a similar modeling of the physical properties of the emission regions in the four MSPs studied above. A summary of the estimated plasma properties for each MSP at its A/R-determined emission height is given in Table 5.²⁰ The cyclotron frequency ν_B is estimated for a secondary plasma Lorentz factor γ_s of 200. The plasma frequency ν_p is estimated for $\gamma_s = 200$ and two values of the overdensity $\kappa = n_s/n_{GJ}$ of 100 and 10^4 , and the curvature frequency ν_{cr} for two values of $\Gamma_s = 300, 600$, the Lorentz factor of the emitting soliton. The radius of the light cylinder is given by $R_{lc} = cP/2\pi$, and the model height of the radio emission r in terms of light-cylinder distance is given by $R = r/R_{lc}$.

The Table 5 values show that the radio frequency is far lower than conservative estimates of the cyclotron, plasma, and curvature frequencies in every case. This in turn demonstrates not only that MSP emission functions physically in a manner that is very similar or identical to slower pulsars, but it also indicates that the mechanism of radiation must be the curvature process and the emitting entities charged solitons as in slower pulsars (Mitra et al. 2016). Very similar conclusions can be reached via the conclusion that the 22.7 ms pulsar J0737–3039A has an emission height of some 9–15 stellar radii (Perera et al. 2014).

7. Conclusions

MSP J0337+1715 together with the other three pulsars studied above apparently show us that some MSPs are capable of core/(double)-cone emission—and thus that the engines of emission in MSPs are not essentially different than those in slower pulsars. In particular, we have been able to estimate the emission heights of the four MSPs using both geometric modeling and A/R, and all indicate that the emission regions lie deep within the larger polar flux tubes of their shallower magnetospheres. We also find as for the slower pulsars that in their radio emission regions the cyclotron, plasma, and curvature-radiation frequencies are much higher than those of

the emitted radiation, strongly arguing for the curvature emission process by charged solitons.

We thank Paul Demorest for assistance in analyzing a Green Bank Telescope observation of B1913+16 and Michael Kramer for use of his bfit code. Much of the work was made possible by support from the US National Science Foundation grant 09-68296 as well as NASA Space Grants. One of us (J.M.R.) also thanks the Anton Pannekoek Astronomical Institute of the University of Amsterdam for their NWO Vidi/Aspasia grant (PI Watts) support. Another (J.v.L.) thanks the European Research Council for funding under Grant Agreement n. 617199. J.M.W. was supported by NSF Grant AST 1312843 Arecibo Observatory is operated by SRI International under a cooperative agreement with the US National Science Foundation, and in alliance with SRI, the Ana G. Méndez-Universidad Metropolitana, and the Universities Space Research Association. The National Radio Astronomy Observatory is a facility of the National Science Foundation operated under cooperative agreement by Associated Universities, Inc. This work made use of the NASA ADS astronomical data system.

Appendix Results of Profile Modeling

A.1. J0337+1715

In order to intercompare our analyses in the four bands conveniently, they should be well aligned in time. An attempt was made to align the profiles according to their timing and dispersion delay, which was roughly satisfactory (except for the 2.0 GHz band, which was found to be early by about 10° , and the 430 MHz band, which was late by about 5°). The adjustments brought the centers of the putative “caustic” features into close alignment, as can be seen in the models of Table 6, and Figure 6 is a check on the Arecibo polarimetry.

Figure 5 shows the 1391 MHz and other profiles with the various model components. Similar modeling efforts were carried out for each of the profiles, and the results are tabulated in Table 6. The inner and outer cones and core are modeled with Gaussian components, and one further Gaussian is used to model the putative caustic component on the trailing edge of the trailing inner conal component. The leading conal components then align within an rms of about a degree, and the trailing ones about twice that. Clearly, the Gaussian functions model the profile components only poorly. Most components have complex and asymmetric shapes, and the

²⁰ Values are also given in italics for B1953+29 and J1022+1001 corresponding to the geometric model (characteristic) heights in Table 4, where the A/R height may only measure the difference between the core and conal emission heights.

Table 6
J0337+1715 Component Modeling Summary

	LOC	LIC	Core	TIC	TOC	“CC”
<i>1.4 GHz Band</i>						
C (°)	-100	-47	83	99	128	110
W (°)	17	18	67.5	20	12	3.5
A	82.0	17.6	14.0	23.1	45.7	14.0
<i>2.8 GHz Band</i>						
C (°)	-105	-51	87	98	124	109
W (°)	19	14	67.5	14	8	4.7
A	0.20	0.06	0.04	0.08	0.10	0.15
<i>2.0 GHz Band</i>						
C (°)	-102	-49	87	97	125	110
W (°)	16	16	67.5	17	13	5.8
A	13.5	3.0	2.2	4.2	5.8	6.0
<i>327 MHz Band</i>						
C (°)	-103	-48	84	94	129	...
W (°)	19	19	67.5	24	21	...
A	940	498	179	150	500	...

Note. “LOC/LIC” leading inner/outer cones; “TIC/TOC” trailing inner/outer cones; and “CC” caustic component. “C” center; “W” half-power width; and “A” amplitude.

fitting results seem adequate only to estimate the widths and centers of the five components approximately.

However, it is the center of the core component that in principle falls close to the magnetic axis, but this point can only be estimated by modeling due to the conflation of the core with the trailing components. In particular, the Gaussian model for the core component’s shape at 1391 MHz is clearly poor. The modeling efforts do show that the space is adequate before and below the trailing components for a core of the expected 67.5 half-width. Recent evidence indicates that some cores may have an unresolved double form, and a model using two Gaussians of half the expected width and separated by this half-width does model the 1391 MHz feature somewhat better (dashed magenta curve).

The Gaussian component modeling of the estimated core centers gives reasonably consistent results for the four bands, as seen again in Figure 5 and Table 6. In each case, the core width was fixed at its expected 67.5 value, and its amplitude was also adjusted to be about 15% of the two leading conal component’s amplitudes in order to control the correlation of its amplitude with that of the trailing inner conal component. Within these assumptions, the estimated core center position falls at $+85^\circ \pm 2^\circ$ longitude. However, the probable errors are much larger. The A/R analysis above uses the differences between the conal component centers and the core center. We have seen that the model differences across the bands of a conal component center are only one or two degrees; however, a different modeling assumption might shift the core center by a larger amount. We therefore propose to adopt a core center value of $+85^\circ \pm 10^\circ$ to accommodate these various uncertainties.

A.2. B1913+16

The binary pulsar B1913+16 can no longer be observed to clearly show its three components and putative core-cone structure at frequencies around 430 MHz. Its secularly changing profiles show that its emission beam is precessing, shifting the orientation of our sightline’s traverse through it, such that

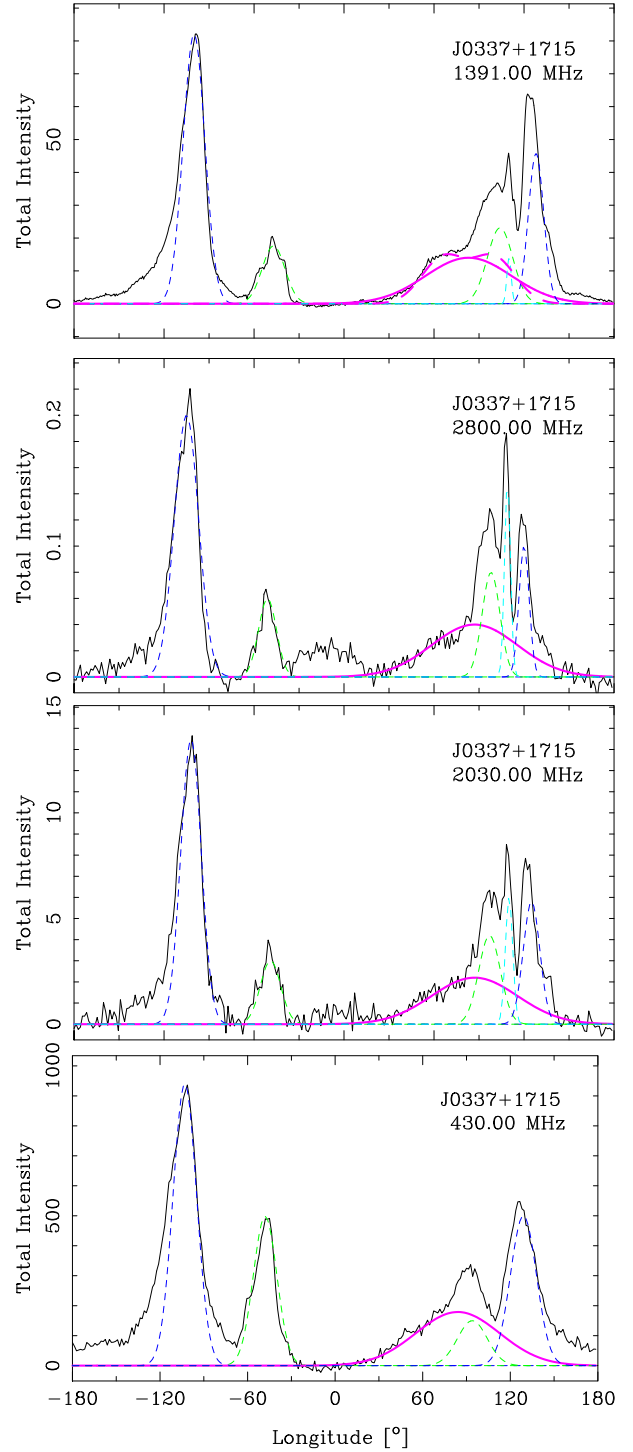


Figure 5. Total power profiles of J0337+1715 as in Figures 1 and 2, showing the several Gaussian functions used to model the profiles and estimate the centers and dimensions of the components in Tables 2, 3, and 6. The outer conal Gaussian functions are shown as a dashed blue line, the inner as a dashed green line, and the core as a solid magenta line—and the caustic feature is plotted as a dashed cyan line. An unresolved double model is also shown for the 1391 MHz profile (dashed magenta); see text. The model dimensions are given in Table 6.

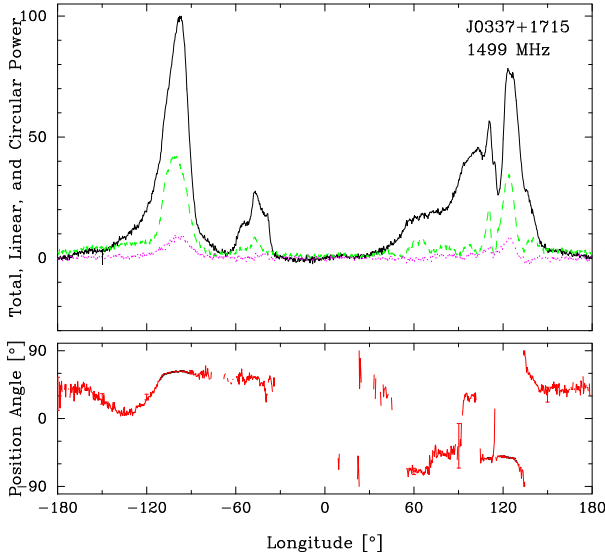


Figure 6. Total 1.4 GHz Green Bank Telescope GUPPI profile of pulsar J0337+1715 as in Figure 1. The profiles compare well with each other, despite concerns that the polarization might be distorted by reflections for a source that must be tracked at Arecibo fully under its triangular supporting structure. The Green Bank Telescope is designed to avoid all such issues. Arecibo’s PUPPI and the latter’s GUPPI are almost identical instruments.

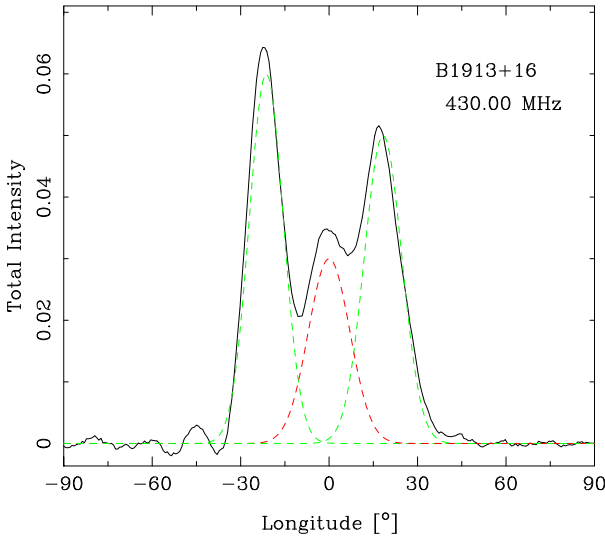


Figure 7. Arecibo 430 MHz profile of B1913+16 from 1990 August 18 showing the three Gaussian functions used to fit the profile and estimate the centers and dimensions of the components in Tables 4 and 7. The conal Gaussian functions are shown as a green line, and the central core is plotted as a red line. The baseline ripples on the leading edge may result from interference.

eventually, its beam will no longer point in our direction (Weisberg & Taylor 2002). Therefore, we make use here of both archival and current observations. Please refer to the well-measured Arecibo profiles of Blaskiewicz et al. (1991; their Figure 17); Figure 3 gives a current Arecibo 1390 MHz profile; and we use another archival Arecibo observation in Figure 7 to determine the centers and widths of its three profile components by Gaussian fitting.

Table 7
Component Fitting Summary for Pulsars B1913+16, B1953+29, and J1022+1001

Pulsar (GHz)		LC (°)	Core (°)	TC (°)	IP (°)
B1913+16	C	-23.8	-2.8	15.8	...
	W	13.6	16.6	15.0	...
	A	0.06	0.03	0.05	...
B1953+29	C	-52.2	-2.8	15.5	-165.6
	W	13.6	16.6	15.0	25.9
	A	132e3	55e3	81e3	9e3
J1022+1001 410 MHz	C	-12.5	0.4	12.5	...
	W	27.9	13.6	6.0	...
	A	0.34	0.77	0.73	...
610 MHz	C	-15.3	3.4	15.1	...
	W	18.9	17.8	5.4	...
	A	0.15	0.59	0.78	...

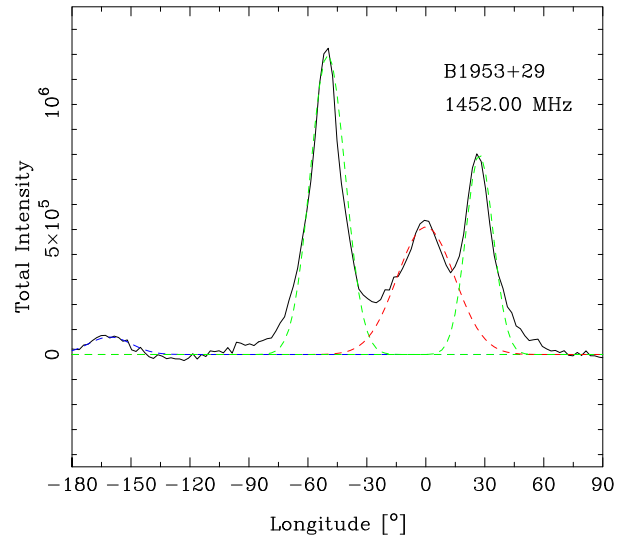


Figure 8. Total power profile of B1953+29 at 1452 MHz as in Figure 3, showing the several Gaussian functions used to fit the profile and estimate the centers and dimensions of the components in Tables 4 and 7. The conal Gaussian functions are shown as a green line, and the central core is plotted as a red line.

The fitting results are given in Table 7. Here the Gaussian fits worked well as can be seen in the figure, implying that here the three components can be closely modeled using Gaussian functions. These dimensions are used above to assess the half-power width of the central components so as to vet it as a core component, and in Table 4 to quantify the geometry of the pulsar’s cone after ET VIa and ET VIb.

A.3. B1953+29

Similar Gaussian fitting was carried out for MSP B1953+29 using the 1452 MHz Arecibo observation in Figure 3 above. The results of the fits for the three profile components and possible interpulse are shown in Figure 8, where it is clear that the modeling was again successful in this case. Gaussian functions fit all four profile features well, and their fitted centers and widths are again given in Table 7. The results are also used above to assess whether the core width is compatible with a

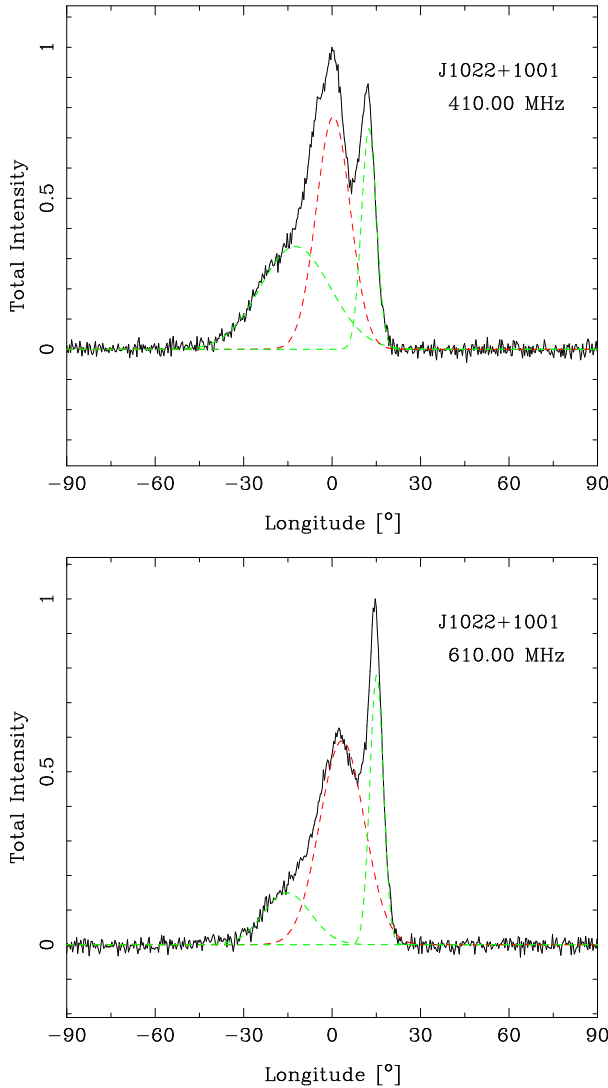


Figure 9. Total power profiles of J1022+1001 at 410 MHz (upper panel) and 610 MHz (lower panel) from Jodrell Bank Observatory, showing the several Gaussian functions used to fit the profile and estimate the centers and dimensions of the components, in Tables 4 and 7. The conal Gaussian functions are shown as a green line, and the central core is plotted as a red line.

core identification and to provide an analysis of the conal beam geometry in Table 4.

A.4. J1022+1001

We also studied the profiles of pulsar J1022+1001. The results of the two fits for the pulsar’s three profile components are given in Figure 9. Gaussian functions fit the three profile features well, and their fitted centers and widths are again given in Table 7. Kramer et al. (1999) fitted the overall pulsar profile at 1.4 GHz with five Gaussian components, and the star’s profile does exhibit a narrow “cap”-like feature at 1 GHz and above somewhat similar to the caustic profile of J0337+1715. Indeed, our observations show that the relative intensity of this narrow “cap” feature increases very rapidly with frequency from being undetectable at meter wavelengths, just so at 1 GHz

and dominant at 1.7 GHz. The alignment of the meter and centimeter profiles is very nicely shown in the recent paper by Noutsos et al. (2015; Figure 11). We therefore conclude that its behavior is unlike anything previously seen in cores and can be ignored for the present purposes. The results are also used above to assess whether the core width is compatible with a core identification and to provide a quantitative analysis of the conal beam geometry in Table 4.

ORCID iDs

Joanna M. Rankin <https://orcid.org/0000-0002-8923-6065>
 Anne Archibald <https://orcid.org/0000-0003-0638-3340>
 Jason Hessels <https://orcid.org/0000-0003-2317-1446>
 Dipanjan Mitra <https://orcid.org/0000-0002-7653-8494>
 Scott Ransom <https://orcid.org/0000-0001-5799-9714>
 Ingrid Stairs <https://orcid.org/0000-0001-9784-8670>
 Willem van Straten <https://orcid.org/0000-0003-2519-7375>
 Joel M. Weisberg <https://orcid.org/0000-0001-9096-6543>

References

- Blaskiewicz, M., Cordes, J. M., & Wasserman, I. 1991, *ApJ*, 370, 643
 Boriakoff, V., Buccheri, R., & Fauci, F. 1983, *Natur*, 304, 417
 Boriakoff, V., Stinebring, V., et al. 1984, NRAO Workshop 8
 Camilo, F., Nice, D. J., Shrauner, J. A., & Taylor, J. H. 1996, *ApJ*, 469, 819
 Clifton, T., & Weisberg, J. M. 2008, *ApJ*, 689, 687
 Dai, S., Hobbs, G., Manchester, R. N., et al. 2015, *MNRAS*, 449, 3223
 Dyks, J. 2008, *MNRAS*, 391, 859
 Dyks, J., & Rudak, B. 2003, *ApJ*, 598, 1201
 Dyks, J., Rudak, B., & Harding, A. K. 2004, *ApJ*, 607, 939
 Force, M. M., Demorest, P., & Rankin, J. M. 2015, *MNRAS*, 453, 4485
 Force, M. M., & Rankin, J. M. 2010, *MNRAS*, 406, 237
 Gangadhara, R. T., & Gupta, Y. 2001, *ApJ*, 555, 31
 Gil, J., Lyubarski, Y., & Melikidze, G. I. 2004, *ApJ*, 600, 872
 Gil, J. A., Kijak, J., & Seiradakis, J. M. 1993, *A&A*, 272, 268
 Goldreich, P., & Julian, W. H. 1969, *ApJ*, 157, 869
 Gonzalez, M. E., Stairs, I. H., Ferdman, R. D., et al. 2011, *ApJ*, 743, 102
 Han, J. L., Demorest, P. B., van Straten, W., & Lyne, A. G. 2009, *ApJS*, 181, 558
 Han, J. L., Manchester, R. N., Lyne, A. G., Qiao, G. J., & van Straten, W. 2006, *ApJ*, 642, 868
 Hotan, A. W., Bailes, M., & Ord, S. M. 2004, *MNRAS*, 355, 941
 Hotan, A. W., van Straten, W., & Manchester, R. N. 2004, *PASA*, 21, 302
 Kondratiev, V. I., Verbiest, J. P. W., Hessels, J. W. T., et al. 2016, *A&A*, 585, 128
 Kramer, M. 1998, *ApJ*, 509, 856
 Kramer, M., Xilouris, K. M., Camilo, F., et al. 1999, *ApJ*, 520, 324
 Kumar, D., & Gangadhara, R. T. 2012, *ApJ*, 746, 157
 Liu, K., Karuppusamy, R., Lee, K. J., et al. 2015, *MNRAS*, 449, 1158
 Malov, I. F., & Suleimanova, S. A. 1998, *ARep*, 42, 388
 Melikidze, G. I., Mitra, D., & Gil, J. 2014, *ApJ*, 794, 105
 Mitra, D., & Deshpande, A. A. 1999, *A&A*, 346, 906
 Mitra, D., Gil, J., & Melikidze, G. I. 2009, *ApJ*, 794, 105
 Mitra, D., Melikidze, G. I., & Gil, J. 2015, in ASI Conf. Ser. 12, Recent Trends in the Study of Compact Objects (RETCO-II): Theory and Observation, ed. I. Chattopadhyay et al. (Bangalore: ASI), 43
 Mitra, D., & Rankin, J. M. 2011, *ApJ*, 792, 92
 Mitra, D., & Rankin, J. M. 2017, *MNRAS*, 468, 4061
 Mitra, D., Rankin, J. M., & Arjunwadkar, M. 2016, *MNRAS*, 460, 3063
 Mitra, D., Rankin, J. M., & Gupta, Y. 2007, *MNRAS*, 379, 932
 Mitra, D., & Seiradakis, J. M. 2004, arXiv:astro-ph/0401335
 Noutsos, A., Sobey, C., Kondratiev, V. I., & Weltevrede, P. 2015, *A&A*, 576, A62
 Perera, B. B. P., Kim, C., McLaughlin, M. A., et al. 2014, *ApJ*, 787, 51
 Ramachandran, R., & Kramer, M. 2003, *A&A*, 407, 1085
 Rankin, J. M. 1983, *ApJ*, 274, 33 (ET I)
 Rankin, J. M. 1993a, *ApJ*, 405, 285 (ET VIa)
 Rankin, J. M. 1993b, *ApJS*, 85, 145 (ET VIIb)
 Rankin, J. M. 2015, *ApJ*, 804, 112

- Ransom, S. M., Stairs, I. H., Archibald, A. M., Hessels, J. W. T., et al. 2014, *Natur*, 505, 520
- Ruderman, M. A. 1991, *ApJ*, 382, 587
- Smith, E. M., Rankin, J. M., & Mitra, D. 2013, *MNRAS*, 435, 1984
- Stairs, I. H., Thorsett, S. E., & Camilo, F. 1999, *ApJS*, 123, 627
- Thorsett, S. E., & Stinebring, D. R. 1990, *ApJ*, 361, 644
- van Straten, W. 2013, *ApJS*, 204, 13
- Weisberg, J. M., & Huang, Y. 2016, *ApJ*, 829, 55
- Weisberg, J. M., & Taylor, J. H. 2002, *ApJ*, 576, 942
- Xilouris, K. M., Kramer, M., Jessner, A., et al. 1998, *ApJ*, 501, 286
- Yan, W. M., Manchester, R. N., & van Straten, W. 2011, *MNRAS*, 414, 2087